The Astrophysical Journal, 687:658–667, 2008 November 1

STUDY OF MAGNETIC CHANNEL STRUCTURE IN ACTIVE REGION 10930

Haimin Wang,[1,2] Ju Jing,[1,2] Changyi Tan,[1,2] Thomas Wiegelmann,[3] and Masahito Kubo[4]

Received 2008 May 5; accepted 2008 July 23

ABSTRACT

The concept of "magnetic channel" was first introduced by Zirin & Wang. They were defined as a series of oppositely directed vertical-field inversions separated by extremely narrow elongated transverse fields. In this paper, we utilized unprecedented filtergraph and spectropolarimetry observations from *Hinode*, and studied the evolution and physical properties of channel structure of AR 10930 in detail. We found the following: (1) Channels are associated with new flux emergence in the middle of existing penumbra connecting the δ sunspot. (2) The width of each channel is in the order of $1''$ or less. (3) The line-of-sight magnetic gradient is highest in the channel, 2.4–4.9 G km^{-1}. (4) The fields are highly sheared and inclined with a median shear angle around 64° and inclination angle around 25°. (5) Using nonlinear force-free field (NLFF) extrapolation, we derive a near surface current system carrying electric current in the order of 5×10^{11} A. (6) The X3.4 flare on 2006 December 13 occurred during the period that the channels rapidly formed, but a few hours before the maximum phase of channel structure development. Based on the observational evidence, we propose that the channels are formed during the emergence of a sequence of magnetic bipoles that are squeezed in the compact penumbra of the δ sunspot and they are highly nonpotential. Formation of channels might be a precursor of major flares.

Subject headings: Sun: activity — Sun: flares — Sun: magnetic fields

1. INTRODUCTION

It is generally known that the magnetic field provides the energy for the solar energetic events, namely, flares and coronal mass ejections (CMEs). Although the details of energy storage and release have not been fully understood yet, from the observational point of view, the frequency and intensity of the activity seen in the solar corona correlate well with the size and complexity of the host active region (Sawyer et al. 1986; McIntosh 1990; Falconer et al. 2003). Those active regions of a nonpotential configuration (i.e., with significant field-aligned currents) can easily store the 10^{30}–10^{33} ergs of energy appropriate for powering flares (Krall et al. 1982; Metcalf et al. 1995, 2005). Schrijver et al. (2005) classified active regions into flare-active and flare-quite regions according to the comparison of extrapolated three-dimensional (3D) potential magnetic fields and *TRACE* coronal loops. Flares are found to occur 2.4 times more frequently in active regions with nonpotential coronae than in near-potential regions, while their average X-ray peak flare brightness is 3.3 times higher. In an effort to identify an activity-productive indicator, numerous photospheric magnetic properties have been explored. For example, based on 18 years of observations, Zirin & Liggett (1987) found that δ sunspots are responsible for almost all great flares. Wang et al. (1994b) first quantitatively studied the evolution of magnetic flux and the vertical current as well as their relationship with the flare activity. Wang et al. (1996) examined the temporal variation of the total vertical current in an active region and suggested that the existence of strong current systems contribute to the flare activity. The importance of magnetic shear to the flare occurrence was first introduced by the MSFC group (e.g., Hagyard et al. 1984). Kurokawa (1987) pointed out that the shear can be developed by two different ways: collision of two sunspots of opposite magnetic polarities and the successive emergence of twisted magnetic flux ropes. Falconer (2001) measured the length of strong-field, strong-sheared neutral line (LSS) and global net current of four active regions and proposed that they might be prospective predictors of the CME productivity of active regions. In addition, Wang et al. (2006) studied the magnetic structure of five active regions that produce great flares and found a positive correlation between the magnetic gradient and magnetic shear. Leka & Barnes (2003a, 2003b, 2007) have addressed potential and limitation of using photospheric magnetic field properties to distinguish flare-productive and flare-quite regions (also see Barnes & Leka 2006; Barnes et al. 2007).

Jing et al. (2006) obtained some preliminary results to demonstrate the feasibility of establishing the relationship between magnetic topology and flare index quantitatively. They started with the parameters that could be derived directly from the line-of-sight magnetograms, such as the length of neutral line with strong line-of-sight magnetic gradient, the mean gradient values of the neutral lines and the photospheric magnetic energy dissipation. They noted that, as the correlation between the 1 day flare index and magnetic parameters is evaluated, predictability of flares based on magnetic energy dissipation and length of neutral line with strong gradient is reasonably high.

The importance of emerging flux regions (EFRs) leading to solar activities was noted more than two decades ago (e.g., Zirin 1983). Tanaka (1991) made some fundamental discovery in investigating the complex subsurface magnetic rope structure of a very flare-active isolated δ group. This group showed unusually fast evolution accompanied by a number of intense flares occurring on the neutral line of the δ spot, and made it possible to study the inherent relation of flare occurrence to changes of the magnetic configuration. The evolution of this isolated δ group is shown to decompose into two flare-associated elementary modes: shearing produced by spot growth, and reduction of shear as spots disappear. A model of an emerging twisted magnetic knot was proposed to explain the observed magnetic field evolution. The inferred magnetic topological structure of this region consists of

[1] Big Bear Solar Observatory, New Jersey Institute of Technology, 40386 North Shore Lane, Big Bear City, CA 92314-9672.
[2] Center for Solar Terrestrial Research, New Jersey Institute of Technology, Newark, NJ 07102.
[3] Max-Planck Institut fuer Sonnensystemforschung, Max-Planck, Strasse 2 37191, Katlenburg-Lindau, Germany.
[4] High Altitude Observatory, National Center for Atmospheric Research, P.O. Box 3000, Boulder, CO 80307.

tightly twisted knots and a long-winding twisted rope with an internally reversed loop and a hooked bottom structure. The abnormal evolution of this δ group was explained by their consecutive emergences. This concept was further explored by Ishii et al. (1998, 2000) and Kurokawa et al. (2002). In particular, Kurokawa et al. (2002) studied the flare-productive AR 9026 for its long-term evolution and found drastic changes in the δ sunspot configuration that started several hours before the big flares. Based on observations, they constructed a schematic model of an emerging twisted flux rope to explain the evolution of photospheric magnetic structure based on magnetic flux change in the whole active region.

Zirin & Wang (1993) found that magnetic flux can emerge inside the penumbrae of existing sunspots. This kind of new flux emergence can produce so-called magnetic channel, which is an elongated magnetic structure with alternating magnetic polarities and strong transverse magnetic fields along the channels (see Fig. 3 of Zirin & Wang). Surface plasma flows are observed along the channels as well. The penumbral flux emergence is also known to be a common property of a few superactive regions, which produced multiple major solar flares, such as NOAA 5395 in 1989 March, NOAA 5629 in 1989 August, NOAA 5747 in 1989 October (see Tang & Wang 1993 for these three regions), NOAA 6659 in 1991 June, and NOAA 9393 in 2001 March/April (Wang et al. 2002; Wang 2005). However, spatial resolution of magnetograms has not been sufficiently high to study the channel structure in detail.

The recently launched *Hinode* satellite provides unprecedented data with high resolution and cadence, which would allow us to study the nature of magnetic channels and their role in powering flares. Kubo et al. (2007) studied the evolution of photospheric magnetic fields in active region 10930 that produced a number of large flares in 2006 December. They focused the study on the magnetic field properties at the site of the X3.4 class flare, using a time series of vector field maps with high spatial resolution. The flare occurred on 2006 December 13 at the apparent collision site between the large, opposite polarity umbrae. Elongated magnetic structures with alternatingly positive and negative polarities resulting from flux emergence appeared one day before the flare in the collision site penumbra. These are direct evidences of magnetic channel structure that was discussed earlier. This active region was further studied by Schrijver et al. (2008), who compared results from 14 nonlinear force-free (NLFF) models. Although the model fields differ markedly, they agree that the strong electrical currents emerge together with magnetic flux proceeding the X3.4 flare. We believe that the magnetic channel is the center part of this current-carrying emerging flux.

In this paper our objective is to study the evolution and properties of these magnetic channels quantitatively, including the electric current system it carries, as well as associated magnetic gradient, magnetic shear and filling factor.

2. DATA DESCRIPTION

Hinode is the follow-up mission to the very successful Japan/UK/US *Yohkoh* mission. The mission consists of a coordinated set of optical, X-ray, and EUV telescopes (Kosugi et al. 2007). The 0.5 m Solar Optical Telescope (SOT) provides angular resolution of $0.2''$–$0.3''$. The focal plane package of SOT consists of Broadband Filter Imager (BFI), Narrowband Filter Imager (NFI), and Spectro Polarimeter (SP). Magnetic fields are measured by the filter vector magnetograph of NFI and by SP. The full field of view is about $320'' \times 160''$ for NFI and SP, and $218'' \times 109''$ for BFI. These data sets are complementary, as filter-based observations provide high-cadence data (1–2 minutes), while spectropolarimeter observations provide high precision in polarization measurements and spectral diagnosis. The spectral resolution of SP is 30 mÅ.

The active region NOAA 10930 appeared on east limb on 2006 December 3. During its disk passage, four X-class flares occurred. the SP of SOT obtained Stokes profiles of two magnetically sensitive Fe lines at 630.15 and 630.25 nm. Photospheric vector magnetograms were derived by Stokes inversion based on the assumption of the Milne-Eddington atmosphere (T. Yokoyama et al. 2008, in preparation). Around the time of the X3.4 flare on December 13, vector magnetograms were observed at three time bins, 20:30–21:33 UT on 2006 December 12, and 04:30–05:36 UT and 12:51–14:17 UT on 2006 December 13. Our study is mainly based on the last data set. The 180° ambiguity in the vector magnetograms is resolved using the the minimum energy algorithm that simultaneously minimizes both the electric current density and the field divergence (Metcalf 1994). This minimum energy algorithm is the top performing automated method among present state-of-art algorithms used for resolving the 180° ambiguity (see Metcalf et al. 2006 for details). The potential fields were computed with the Green's function method (Metcalf et al. 2008). The magnetogram data and the potential fields for the first two time bins were prepared for the NLFFF-consortium (Schrijver et al. 2008). The same procedures were followed when we processed the data set of the third time bin. The details of the data preparation including remapping and disambiguation are described by Schrijver et al. (2008). However, to study the fine structure of magnetic fields in this paper, we did not rebin the magnetograms, and kept the original pixel size of $0.16''$ for the extrapolation. Because of the computation limitation, we have to limit the field of view to the size of the active region, i.e., about $70'' \times 70''$. In order to reduce the effect of the Lorentz force acting in the photosphere and find suitable boundary conditions for the NLFF field extrapolation, the photospheric vector magnetograms have been preprocessed using a method devised by Wiegelmann et al. (2006).

Besides the high-precision SP vector magnetogtrams, we also used SOT/NFI magnetograms to take the advantage of the high cadence. We analyzed available *Hinode* filtergraph data from 00:00 on 2006 December 11 to 23:00 on December 14 (UT). The G-band (430 nm) observations were obtained with the BFI with a 2 minute cadence. High-cadence observations from the *Hinode* filtergraph observations are essential to detect and characterize the rapid structural changes in sunspots. However, *Hinode* SOT/NFI has some technical difficulties that preclude vector magnetograph observations, only Stokes V images at 120 mÅ in the blue wing of Fe I λ6302 are available that are proportional to line-of-sight magnetic flux density in the weak field regime. Therefore they are only useful for the morphological study. On the other hand, analyzing lower cadence *Hinode* spectropolarimeter observations enables us to study the structure of vector fields at selected times as discussed above.

3. OBSERVATIONAL FINDINGS

The primary objective of this study is to investigate the spatial structure and the development of the magnetic channels. Figure 1 shows a sequence of NFI Stokes V images. The movie of magnetic flux density images derived from SP demonstrated the high dynamics of the region characterized by flux emergence and twisting motion, as described by Kubo et al. (2007). Zhang et al. (2007) also studied the sunspot rotation of this active region using MDI data. The visual inspection shows the development of the channel structure started in the middle of December 11 (marked by an oval) and vanished at the end of December 13,

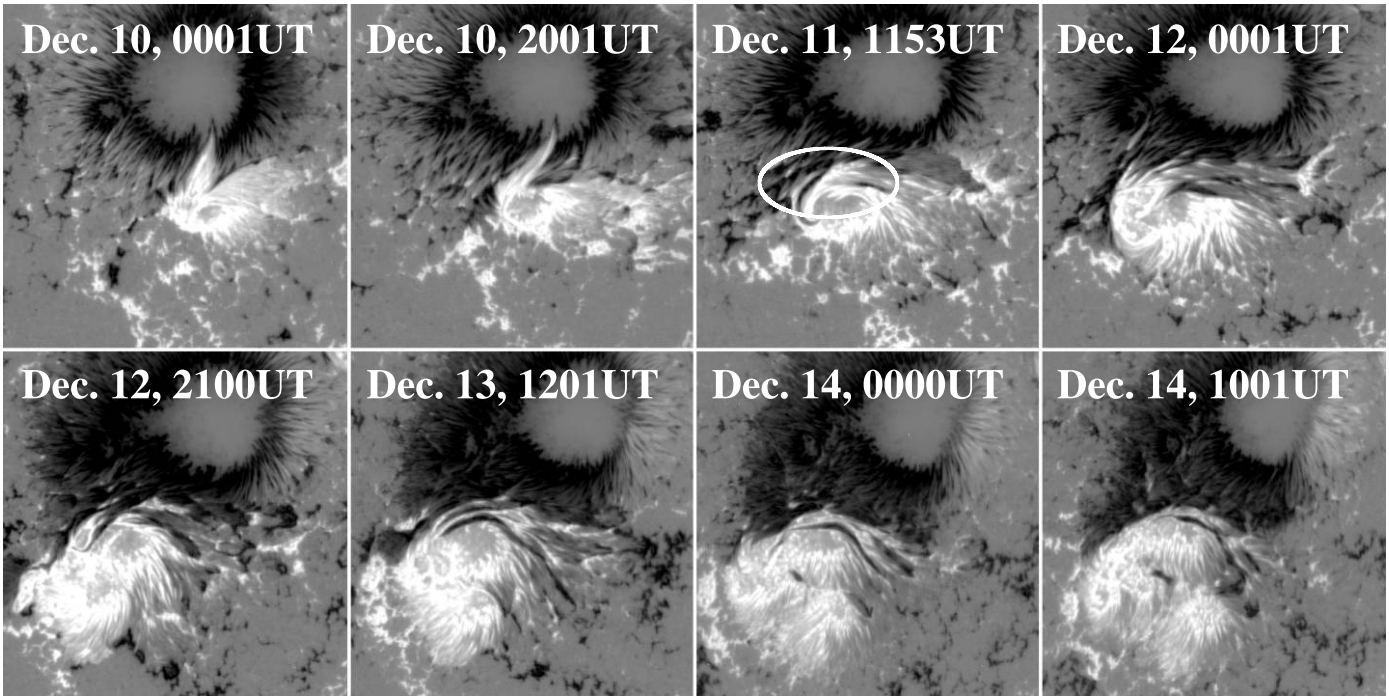

FIG. 1.—Time sequence of Stokes *V* images obtained by *Hinode* NFI system from 00:00 on December 10 to 10:00 on 2006 December 14 (UT). The field of view (FOV) is $80'' \times 80''$ An oval in the panel of December 11 marks the location and start time of channel formation.

while the X3.4 occurred at 02:00 on December 13 (UT). Some isolated elongated structures with negative polarity appear before and after the period of rapid channel development. We believe that they are different from channels, as they are not highly dynamic. They may be classified as parasitic magnetic configuration (e.g., Wang et al. 1999).

Figure 2 shows the magnified line-of-sight magnetogram that was obtained by SP and the corresponding G-band image at the peak development of the channel around 12:00 on December 13 (UT). The vertical line in each panel marks the most prominent part of the channels. Five magnetic neutral lines (also called polarity inversion line) are visible corresponding to four alternating elongated magnetic channels. G-band image shows that the fields are highly sheared as the fibrils are parallel to the direction of magnetic neutral line.

It is obviously that channel structure can be characterized by occurrence of extra magnetic neutral lines. Therefore, following the method of Song et al. (2008) and Jing et al. (2006), we use the length of a high-gradient neutral line to demonstrate the complexity of magnetic topology in the area of the magnetic channels. The top panel of Figure 3 plots the length of neutral line with gradient ≥ 0.1 G km^{-1}, as a function of time. The time of the X3.4 flare is marked by the vertical line. The length of strong gradient neutral lines is distinctly enhanced between 20:00 on

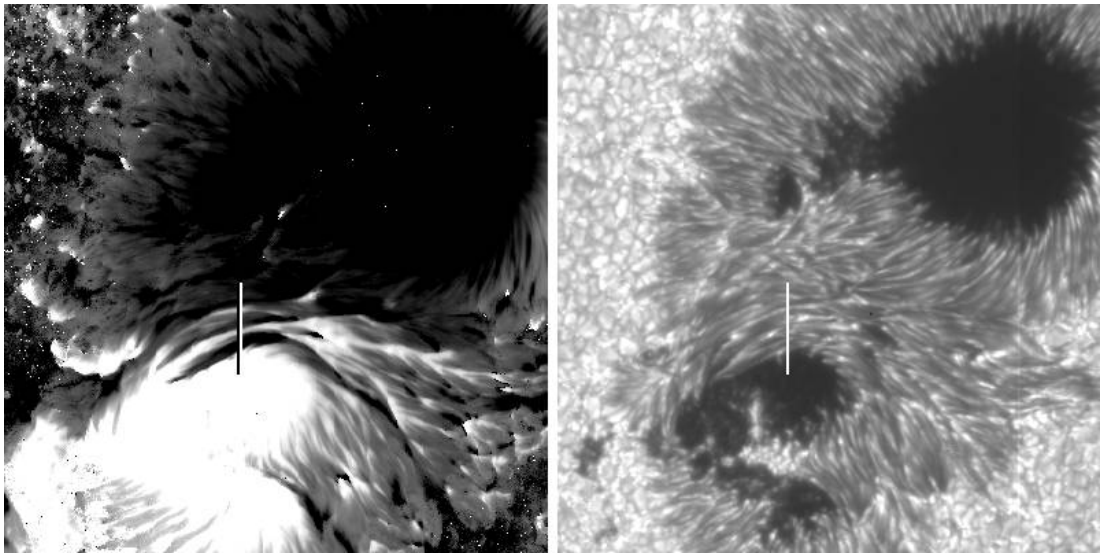

FIG. 2.—Comparison of SOT/SP image of line-of-sight magnetic flux density scanned from 12:51 to 14:17 on December 13 (UT), when the channel structure is most obvious. The FOV is $48'' \times 48''$. The vertical line in each panel marks the center of the channel structure.

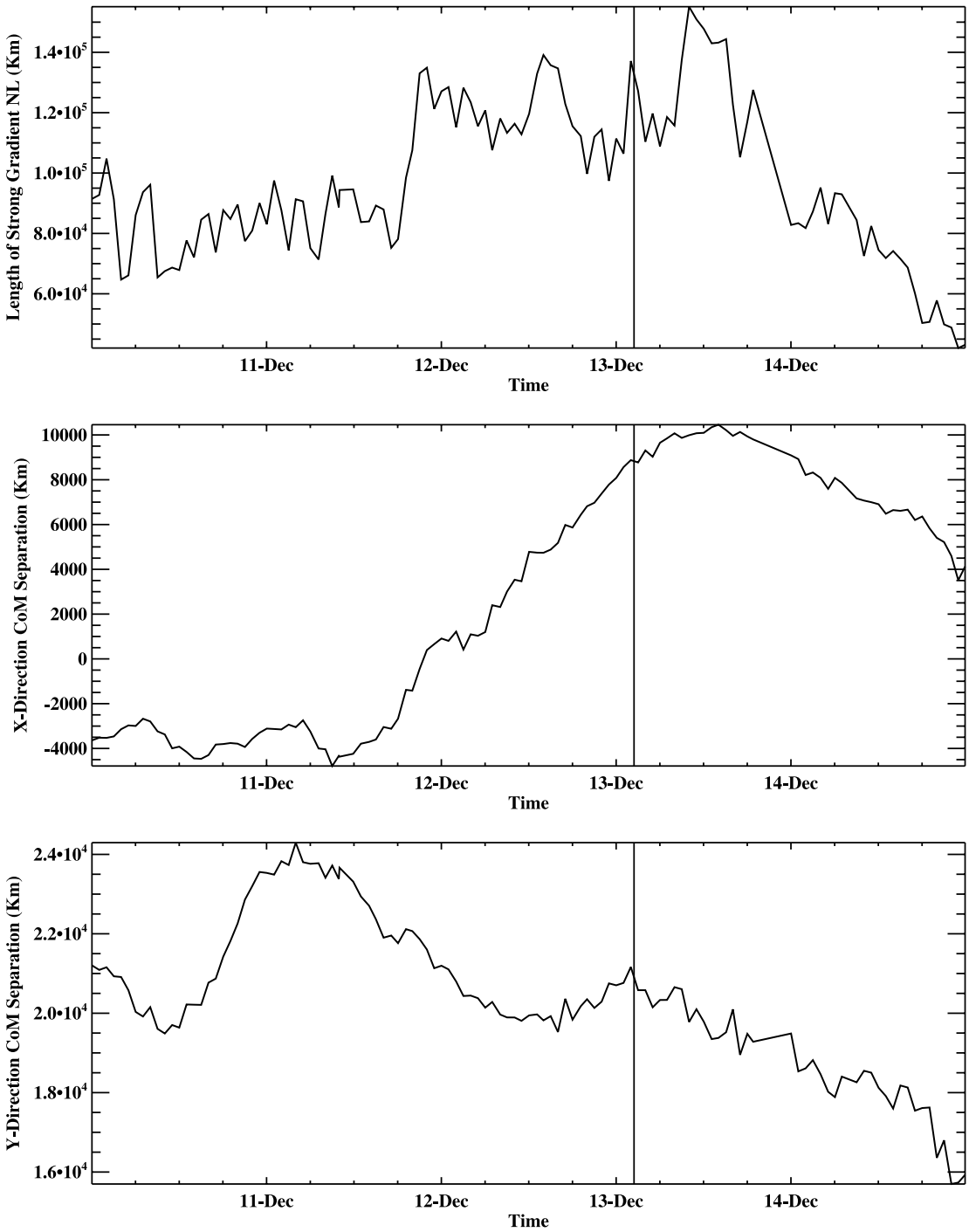

FIG. 3.—Time profiles of the length of strong gradient (≥ 0.1 G km^{-1}) neutral line and the center of mass separation in *X*- and *Y*-directions. These are based on NFI observations.

December 11 and 00:00 on December 14 (UT), so the length of gradient neutral line would be a vital indicator of formation of channel structure. Abramenko et al. (2008) studied the intermittency of the same active region based on the analysis of spatial power spectra. They found that the intermittency peaked about 30 hr (i.e., also around 20:00 on December 11 [UT]) before the occurrence of the X3.4 flare. It is reasonable to assume that such a intermittence enhancement reflects the formation of magnetic channel structure as well.

The bottom two panels of Figure 3 demonstrate the large-scale sunspot motion associated with the flare. We use the center-of-mass (COM) concept to measure the position of positive and negative pixels weighted by the magnetic flux density of each pixel (Wang 2006). In *X*-direction, positive COM separation means that the mean positive flux is in the east of negative flux; in *Y*-direction, positive COM separation means that the mean positive flux is in the south of negative flux. The measurement is not accurate as the flux density in the sunspot umbra is not measurable with NFI Stokes *V* images. Nevertheless, the trend of sunspot motion can be demonstrated by these time profiles. In general, the magnetic neutral line of this sunspot is in the horizontal direction (*X*-direction). Therefore, we separately study

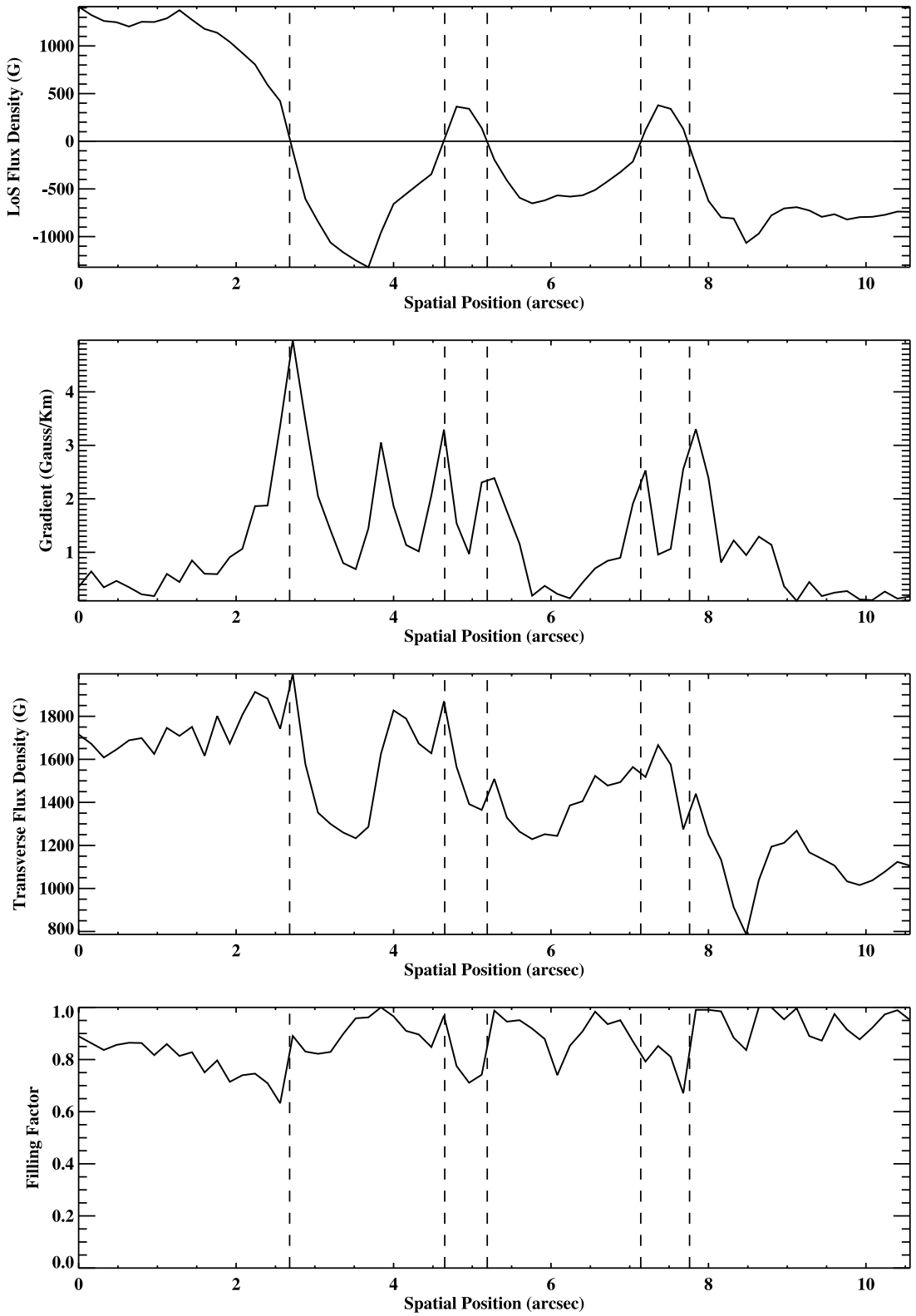

FIG. 4.—Spatial profiles of line-of-sight magnetic flux density, gradient based on line-of-sight flux density and transverse field across the channel system, along the line shown in Fig. 2. Five dashed vertical lines show the position of five identified neutral lines from SP line-of-sight magnetic field measurement. The filling factor is plotted in the bottom panel. This SP time bin corresponds to the maximum development phase of the channel structure.

the *X*- and *Y*-direction motions. The increase/decrease in the *X*-direction COM separation represents shear/de-shear motion, while the increase/decrease in *Y*-direction COM separation represents diverging/converging motion. From the second panel of Figure 3, the shear motion started around 12:00 on December 11 and ends around 14:00 on December 13 (UT), coinciding with the duration of magnetic neutral line enhancement. The speed of this motion is around 0.1 km s^{-1}. Therefore, we believe that the shear motion is closely associated with the formation of the magnetic channel structure. On the other hand, starting from 00:00 on

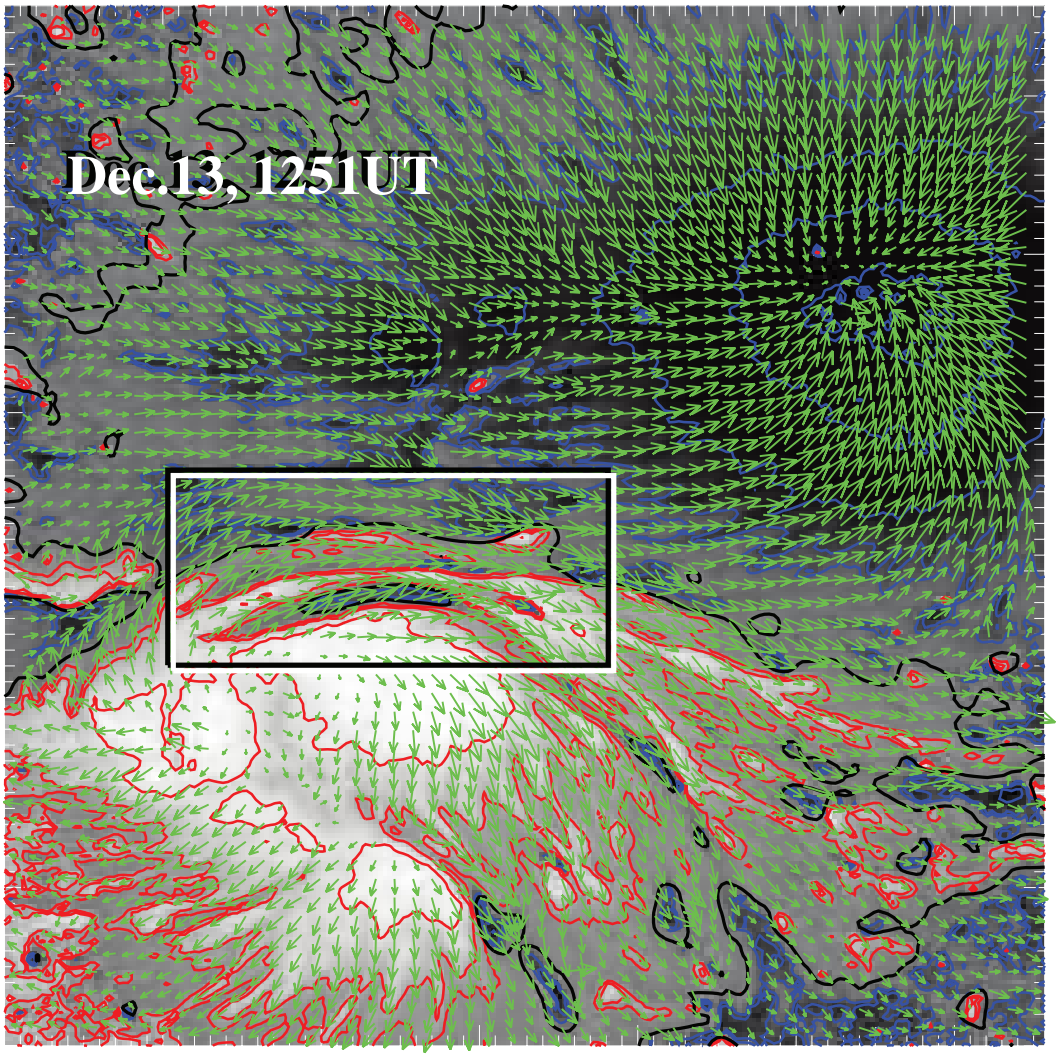

FIG. 5.—SP vector magnetogram corresponding to the line-of-sight magnetogram shown in Fig. 2. Green arrows indicate the transverse fields. Red and blue contours show negative and positive line-of-sight magnetic field strength, respectively. The thick, solid black lines are the neutral lines of the line-of-sight magnetic field. The FOV is $66'' \times 66''$. The area around the channel structure is marked with the rectangle.

December 11 (UT), the converging motion is visible as shown in the bottom panel of Figure 3, with a speed of 0.03 km s^{-1}. However, this motion paused for about 10 hr before the flare and continued immediately after the flare. The relation of converging motion to the formation of channel is not as obvious as the shear motion. Taking these motions as boundary condition, P. F. Chen et al. (2008, in preparation) are carrying out a comprehensive modeling of the formation of channel under the observed shear and converging flows, in combination with flux emergence. Their initial result has demonstrated the importance of the shear flow in this process.

To quantitatively analyze the spatial structure of the magnetic channels, we cut through the most prominent part of channels in the direction perpendicular to the orientation of the channels, as delineated by the black/while line in Figure 2. The profiles of line-of-sight magnetic flux density derived by SP and its gradient along this line are plotted in Figure 4. The FWHM of one magnetic polarity in the individual lane is between $0.6''$ and $1.1''$. Five neutral lines with peak gradient between 2.4 and 4.9 G km^{-1} are prominently demonstrated in the bottom plot. Please note that these gradient values are much higher than the previous measurements based on MDI data (e.g., Song et al. 2006; Wang, 2006). This is due to two factors: more accurate Stokes inversion and higher spatial resolution of *Hinode* SP comparing to MDI. As the pixel resolution of the SP magnetograms is $0.16''$, corresponding to a 0.32 spatial resolution, it is possible that even narrower channel structure may be uncovered when the resolution of observation improves, such as with future observations from the 1.6 m New Solar Telescope at BBSO and 4 m Advanced Technology Solar Telescope. Please also pay attention to the strong transverse fields corresponding to the strong gradient, their flux density values are between 1500 and 1800 G, in agreement with what was described by Zirin & Wang (1993). The Stokes inversion also gives the filling factor for each pixel, that is, the ratio between flux density and field strength. The filling factor of the area around the channel is between 0.7 and 1.0, indicating that measured flux density is close to actual field strength.

As we discussed above, although SP data has poor temporal resolution in this observing run, it provides an accurate snap shot measurement of vector fields with high resolution. Figure 5 shows the vector magnetogram corresponding to the line-of-sight magnetogram in Figure 2. The green arrows indicate the

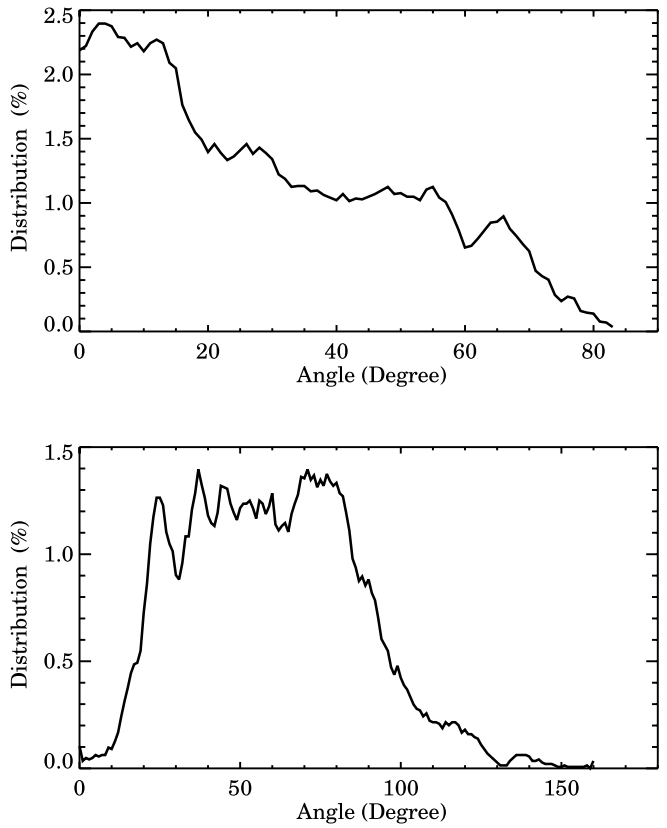

FIG. 6.—*Top*: Distribution of inclination angles in the channel area (marked in Fig. 5). *Bottom*: Distribution of shear angles in the same channel area.

transverse magnetic fields, and the red and blue contours show negative and positive line-of-sight magnetic field strength, respectively. The thick, solid black lines are the neutral lines of the line-of-sight magnetic field. It is obvious that the transverse fields are along the direction of the channel and therefore strongly sheared. An area around the magnetic channels is marked with a rectangle. Figure 6 shows the distribution of inclination and shear angles in this channel area. The inclination angle is defined such that the vertical field lines have a value of 90° and the horizontal field lines have a value of 0°. The shear angle is defined as the azimuth difference between the measured magnetic fields and the potential fields. The median value of inclination angles are 25.5° and that of shear angle is 63.9°. These structures are highly inclined to the vertical and are strongly sheared, confirming the qualitative results of Zirin & Wang (1993). Please note that while calculating these angles, projection effect has been corrected to view the region in heliocentric coordinate system. In Zirin & Wang paper, they found the plasma flow along the channel, such a flow is also present (Tan et al. 2008), in the order of 0.5 km s^{-1}.

The knowledge of the 3D magnetic fields from photosphere to corona is essential for understanding the role of magnetic channel in powering solar flares. The NLFF magnetic fields are computed with the "optimization method" (Wheatland et al. 2000) as implemented by Wiegelmann (2004), using the magnetogram in Figure 5 as the boundary condition. This method is to minimize a joint measure for the normalized Lorentz force and the divergence of the field. After the 3D field structure is extrapolated, the electrical current in the entire coronal volume is derived. The left panel of Figure 7 shows 3D visualization the electric current densities over the active region NOAA 10930 at 12:00 on December 13 (UT). The cutaway view in the right panel displays the interior structure of the current system. The line-of-sight magnetogram is placed as the bottom surface. The magnitude of current densities is indicated by the color bar. Red shows where the electric current densities are highest. In agreement with Schrijver et al. (2008), who used two vector magnetograms earlier than what is used here, we see that strong electric currents ($\geq$0.05 A m^{-2}) are composed mainly of two systems, a low-lying system lies (*indicated by arrow L*) and a higher one (*indicated by arrow H*). The low-lying current system is parallel to the direction of channel structure, while the higher one connects the opposite-polarity penumbrae. This is not surprising as the force-free condition requires the current to be along the direction of magnetic field. We integrated the currents over the lowest 1.5 Mm. The total currents in this lower system is estimated to be in the order of $5.0 \pm 1.0 \times 10^{11}$ A, in the same order of magnitude as was found by previous observations of vertical current (e.g., Leka et al. 1996).

To demonstrate the relationship between the current system and magnetic structure we overlay the extrapolated field lines on the line-of-sight magnetic fields of the photosphere and electric current density at a height of 1.28″, and show in Figure 8. In addition, we show the extrapolated line-of-sight magnetic fields at

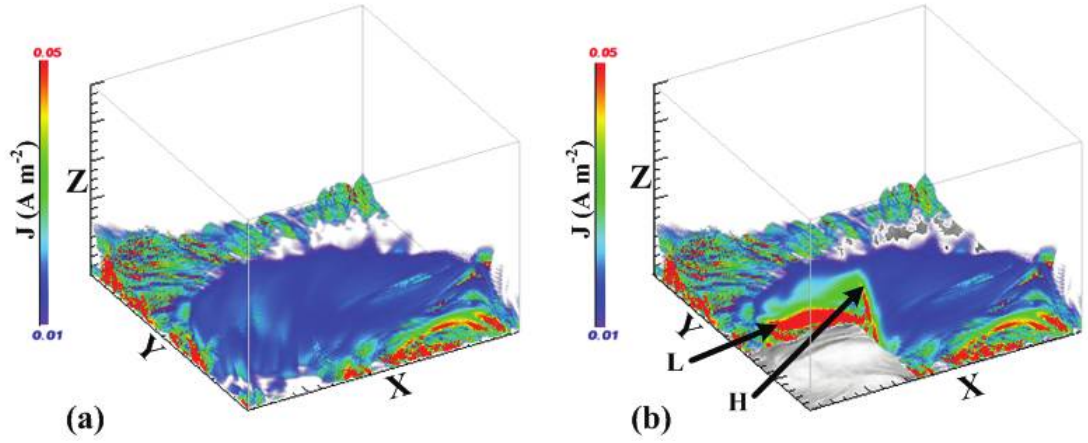

FIG. 7.—(*a*) 3D visualizations of the electric current density over the active region. (*b*) Cutaway view of panel *a*. The corresponding line-of-sight magnetogram is displayed as the bottom surface. Arrows L and H indicate the low-lying and high-arching strong current system, respectively. The dimensions of the simulation box are $66'' \times 66'' \times 30''$.

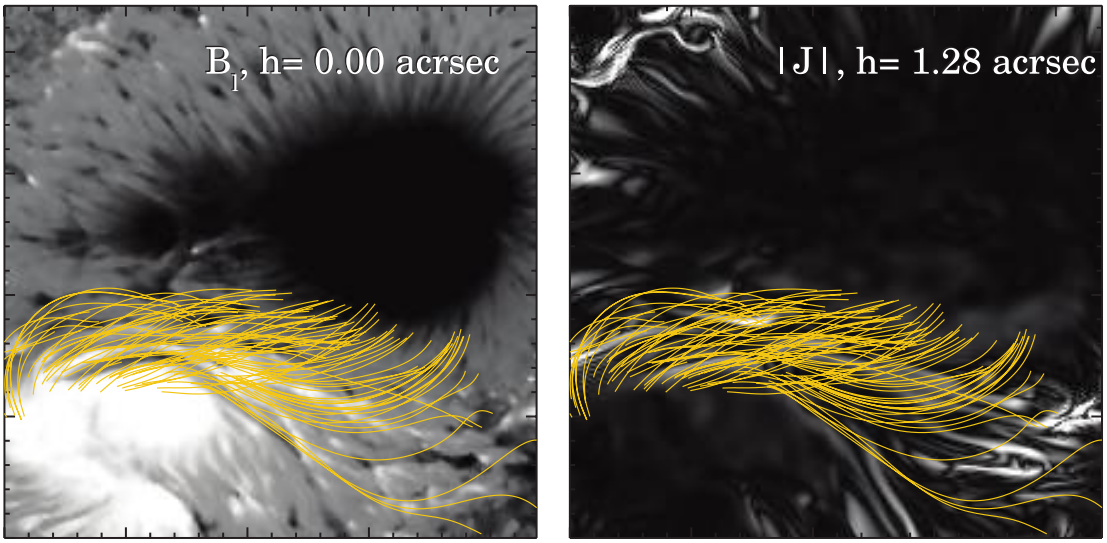

FIG. 8.—*Left*: Line-of-sight magnetic field taken from 12:51 to 14:17 on December 13 (UT). *Right*: Electric current density at a height of 1.28″. The NLFF field lines around the magnetic channel structure are overlaid. The FOV is 66″ × 66″.

several heights in Figure 9. The same figure also shows profiles of line-of-sight magnetic flux density, along the line shown at the top panels, at several heights. Figures 8 and 9 demonstrate the following two properties of the channel. (1) Strongly sheared fields and electric current are closely associated in the channel structure. This may not be surprising, as the extrapolation is based on force free extrapolation, i.e., the fields and currents are along the same direction. In our case, they are dominantly in the horizontal direction. (2) Channel structure is a near-surface (may be subsurface) structure. The mixed polarity properties weaken quickly, even at a height of 500 km above the surface. Therefore, channel structure may not store large amount of energy to power the flare, however, it may be important for the instability to trigger the energy release above the surface.

4. SUMMARY AND DISCUSSION

In this paper we utilized unprecedented filtergraph and spectropolarimetry observations from *Hinode*, and studied the evolution and physical properties of channel structure of AR 10930 in detail. We found the following: (1) Channels are associated with new flux emergence in the middle of existing penumbra connecting the δ sunspot. (2) The width of each channel is in the order

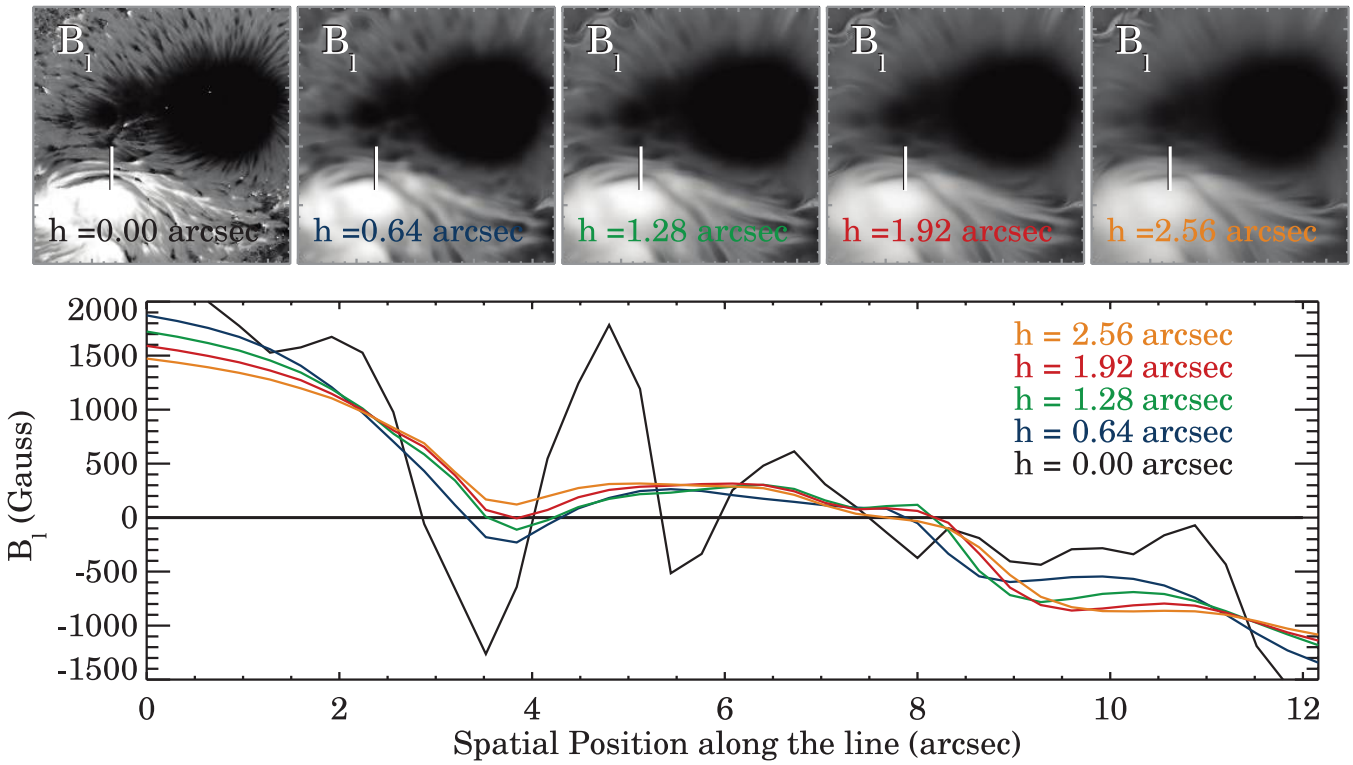

FIG. 9.—*Top panels*: Extrapolated line-of-sight magnetic fields at several heights. The FOV is 66″ × 66″. The vertical line in each panel across the magnetic channel structure is defined for the bottom panel in this figure. *Bottom*: Profiles of line-of-sight magnetic flux density, along the line shown at the top panels, at several heights.

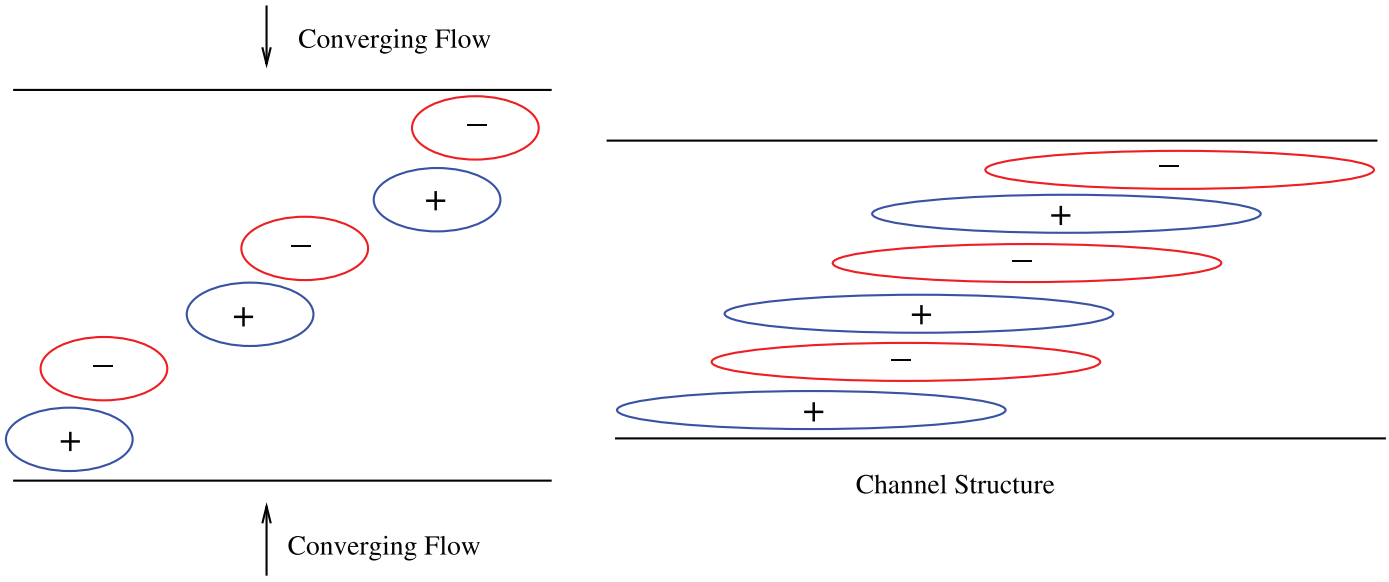

FIG. 10.—Cartoon to demonstrate a possible way to form the channel structure. *Left*: Three pairs of new emergence that may come out at different times. *Right*: The *Y*-direction converging motion plus the *X*-direction separation motion of each dipole form elongated structure with alternating magnetic polarities.

of 1″ or less. (3) The line-of-sight magnetic gradient is highest in the channel, about 2.4–4.9 G km^{-1}. (4) The fields are highly sheared and inclined with a median shear angle around 64° and inclination angle around 25°. (5) Using NLFF extrapolation, we derive a near surface current system carrying an electric current in the order of 5×10^{11} A. (6) The X3.4 flare on 2006 December 13 occurred during the period that the channels rapidly formed, but a few hours before the maximum phase of channel structure development.

It is important to understand the physical source of the channel structure. From the study of the SOT NFI Stokes *V* movie, it is obvious that the channel structure is related to new flux emergence. The X3.4 flare is clearly associated with the occurrence of the channel—it occurred hours after the channel started to form and development of channel continues a few hours after the flare. Magara (2006) modeled the emergence of highly twisted flux tubes. These tubes should carry significant amount of electric currents, and have strong magnetic shear as the observations demonstrate. However, alternating polarities of line-of-sight magnetic structure in small scale cannot be explained by this model alone. Here we propose an explanation that might be combined with the Magara model. As we show in Figure 10, the channel is formed due to emergence of a series of small bipoles. Of course, each bipolar emergence may carry twist and current, as Magara (2006) explained. The emerged bipoles become squeezed and then reformed due to compactness of the emergence to form these elongated structures. If these emergences start in a quite region, segregation motion would simply joint bipoles into leading and following sunspots. In the case as we observed, the emergences are confined by already compacted penumbral structure dividing two polarities, and therefore elongated structures form. As we discussed in several previous papers (e.g., Wang et al. 1994a, 2002), the transverse magnetic fields may increase rapidly after the major flares. This can be explained in the way that the flare removed tight fields in the corona, made it easier for new flux to emerge above the surface. As we mentioned earlier, P. F. Chen et al. (2008, in preparation) are carrying out quantitative modeling to incorporate flux emergence, shear/converging flows to interpret the formation of the channel structure.

Alternatively, we can use the concept of Kurokawa et al. (2002), who demonstrated that the formation of complex δ sunspot is due to emergence of twisted flux tube. Although Kurokawa's picture is for the large-scale structure of the active region, in our case here, if the twisted flux rope is broken into branches of small flux ropes during the emergence, they may form a series of magnetic channels due to kink instability.

We thank the referee for many valuable comments that helped us to improve the paper substantially. The work is supported by NSF under grants ATM 07-45744 and ATM 05-48952, and by NASA under grants NNX07AH78G, NNX08AJ23G, and NNX08AQ90G. *Hinode* is a Japanese mission developed and launched by ISAS/JAXA, with NAOJ as domestic partner and NASA and STFC (UK) as international partners. It is operated by these agencies in cooperation with ESA and NSC (Norway). This work was (partly) carried out at the NAOJ *Hinode* Science Center, which is supported by the Grant-in-Aid for Creative Scientific Research "The Basic Study of Space Weather Prediction" from MEXT, Japan (PI: K. Shibata), generous donations from Sun Microsystems, and NAOJ internal funding.

REFERENCES

Abramenko, V., Yurchyshyn, V., & Wang, H. 2008, ApJ, 681, 1669
Barnes, G., & Leka, K. D. 2006, ApJ, 646, 1303
Barnes, G., Leka, K. D., Schumer, E. A., & Della-Rose, D. J. 2007, Space Weather, 4, 23
Falconer, D. A. 2001, J. Geophys. Res., 106, 25185
Falconer, D. A., Moore, R. L., & Gary, G. A. 2003, J. Geophys. Res. Space Phys., 108, 1380
Hagyard, M. J., Moore, R. L., & Emslie, A. G. 1984, Adv. Space Res., 4, 71
Ishii, T., Kurokawa, H., & Takeuchi, T. 1998, ApJ, 499, 898
———. 2000, PASJ, 52, 337
Jing, J., Song, H., Abramenko, V., Tan, C., & Wang, H. 2006, ApJ, 644, 1273
Kosugi, T., et al. 2007, Sol. Phys., 243, 3
Krall, K. R., Smith, J. B., Jr., Hagyard, M. J., West, E. A., & Cummings, N. P. 1982, Sol. Phys., 79, 59
Kubo, M., et al. 2007, PASJ, 59, S779
Kurokawa, H. 1987, Sol. Phys., 113, 259

Kurokawa, H., Wang, T., & Ishii, T. T. 2002, ApJ, 572, 598
Leka, K. D., & Barnes, G. 2003a, ApJ, 595, 1277
———. 2003b, ApJ, 595, 1296
———. 2007, ApJ, 656, 1173
Leka, K. D., Canfield, R. C., McClymont, A. N., & van Driel-Gesztelyi, L. 1996, ApJ, 462, 547
Magara, T. 2006, ApJ, 653, 1499
McIntosh, P. S. 1990, Sol. Phys., 125, 251
Metcalf, T. R. 1994, Sol. Phys., 155, 235
Metcalf, T. R., Jiao, L., McClymont, A. N., Canfield, R. C., & Uitenbroek, H. 1995, ApJ, 439, 474
Metcalf, T. R., Leka, K. D., & Mickey, D. L. 2005, ApJ, 623, L53
Metcalf, T. R., et al. 2006, Sol. Phys., 237, 267
———. 2008, Sol. Phys., 247, 269
Sawyer, C., Warwick, J. W., & Dennett, J. T. 1986, Solar Flare Prediction (Boulder: Colorado Assoc. Univ. Press)
Schrijver, C. J., DeRosa, M. L., Title, A. M., & Metcalf, T. R. 2005, ApJ, 628, 501
———. 2008, ApJ, 675, 1637
Song, H., Yurchyshyn, V., Yang, G., Tan, C., Chen, W., & Wang, H. 2006, Sol. Phys., 238, 141
Song, H., et al. 2008, Sol. Phys., submitted
Tan, C., Chen, P. F., Abremenko, V., & Wang, H. 2008, ApJ, submitted
Tanaka, K. 1991, Sol. Phys., 136, 133
Tang, F., & Wang, H. 1993, Sol. Phys., 143, 107
———. 2005, ApJ, 618, 1012
———. 2006, ApJ, 649, 490
Wang, H., Chae, J., Qiu, J., Lee, C., & Goode, P. R. 1999, Sol. Phys., 188, 365
Wang, H., Ewell, M. W., Zirin, H., & Ai, G. 1994a, ApJ, 424, 436
Wang, H., Song, H., Jing, J., Yurchyshyn, V., Deng, Y., Zhang, H., Falconer, D., & Li, J. 2006, Chinese J. Astron. Astrophys., 6, 477
Wang, H., Spirock, T. J., Qiu, J., Ji, H., Yurchyshyn, V., Moon, Y., Denker, C., & Goode, P. R. 2002, ApJ, 576, 497
Wang, J., Shi, Z., Wang, H., & Lue, Y. 1996, ApJ, 456, 861
Wang, T., Xu, A., & Zhang, H. 1994b, Sol. Phys., 155, 99
Wheatland, M. S., Sturrock, P. A., & Roumeliotis, G. 2000, ApJ, 540, 1150
Wiegelmann, T. 2004, Sol. Phys., 219, 87
Wiegelmann, T., Inhester, B., & Sakurai, T. 2006, Sol. Phys., 233, 215
Zhang, J., Li, L., & Song, Q. 2007, ApJ, 662, L35
Zirin, H. 1983, ApJ, 274, 900
Zirin, H., & Liggett, M. A. 1987, Sol. Phys., 113, 267
Zirin, H., & Wang, H. 1993, Nature, 363, 426